Available online at www.sciencedirect.com
ScienceDirect
Ceramics International 37 (2011) 3397–3403
CERAMICS INTERNATIONAL
www.elsevier.com/locate/ceramint

Influence of an In_2O_3 buffer layer on the properties of ITO thin films

Boen Houng [a,*], Su Lu Lin [a], Sih Wei Chen [a], Adam Wang [b]

[a] Department of Materials Science and Engineering, I-Shou University, Kaohsiung City 840, Taiwan
[b] Emerging Display Technologies Corp, Kaohsiung City 811, Taiwan

Received 30 March 2011; received in revised form 26 May 2011; accepted 30 May 2011
Available online 6 June 2011

Abstract

In the present study, an indium oxide (In_2O_3) thin film was deposited as a buffer layer between ITO (indium tin oxide) and PES (polyestersulfone) by RF (radio frequency) magnetron sputtering at room temperature, and X-ray diffraction (XRD) and field emission scanning electron microscopy (FESEM) were conducted to characterise the structural variation. The random texture of the ITO/In_2O_3 multilayered film favoured the (2 2 2) crystallographic plane rather than the (4 0 0) plane, which was favoured in single-layer ITO films. Transmission electron microscopy (TEM) observations further indicated that the buffer layer of In_2O_3 film was amorphous, while the ITO film was characterised by a columnar structure that was oriented perpendicular to the substrate surface. The electrical and optical properties of ITO/In_2O_3 multilayered films were enhanced due to the superior crystallinity and larger grain size of the material, as observed by XRD and FESEM. The multilayered film presented an electrical resistivity of $3.1 \times 10^{-4}\ \Omega$ cm, which is significantly better than that of a single-layer ITO film without an In_2O_3 buffer layer ($4.7 \times 10^{-4}\ \Omega$ cm). In addition, optical transmission through the multilayered film increased by 2–4% due to the widening of the band gap by 0.2 eV, which was attributed to a Burstin–Moss shift.

Keywords: ITO; Sputtering; Crystallinity; Multilayered thin films

1. Introduction

In 1907, cadmium oxide (CdO) thin films were first reported to act as transparent conductors. Since then, transparent conducting oxide (TCO) films have attracted a considerable amount of interest in optoelectronic applications [1–3], as evidenced by the wide variety of TCOs that have been produced and the array of techniques developed for their deposition. Currently, tin-doped indium oxide (ITO) is the most successful TCO film, presenting minimum resistivities of 1.0–$1.2 \times 10^{-4}\ \Omega$ cm for commercial products. Recently, indium tin oxides with improved properties have been intensely investigated, including the application of new deposition techniques such as ion-beam-assisted deposition [4], pulsed laser deposition [5] and the use of ultra high density ITO targets [6]. Nevertheless, the electrical conductivities of impurity-doped In_2O_3 thin films have not increased substantially due to the use of these techniques. Many optoelectronic applications rely on high performance ITO films, and the fabrication of TCOs with strong electrical properties is of technical significance. Substrates used in flexible electronic displays, solar cells and electrochromic devices are plastic-based materials; thus, low deposition temperatures are required [7–9]. Compared to glass substrates, plastic substrates offer many advantages such as low weight, durability and easy scale-up. Due to the flexibility of plastic substrates, the shape of the device can be varied to optimise visibility and suppress reflections. Wide viewing angles can be obtained due to the thinner construction of plastic substrates, and the cost of raw materials and mass roll-to-roll production of plastic substrates will likely decrease in the near future. Plastic substrate materials commonly used in display devices include polyethylene terephtalate (PET), polycarbonate (PC), polyarylate (PAR), polyestersulfone (PES), polyimide (PI) and polyolefin. Among the aforementioned materials, PES displays superior optical properties and is low in cost; thus, PES is the most promising substrate for flexible display applications.

By controlling the film thickness, high optical transmission can be achieved while retaining low sheet resistance. The electrical properties of TCO films can be altered to optimise the

* Corresponding author. Tel.: +886 76579708; fax: +886 76578444.
E-mail address: boyen@mail.isu.edu.tw (B. Houng).

0272-8842/$36.00
doi:10.1016/j.ceramint.2011.05.142

response time or minimise the overall device dimensions. To fulfil application requirements, electron degeneracy in wide-gap oxides (>3 eV) can be created by introducing dopants or changing the stoichiometry. However, high donor concentrations result in a distorted crystal lattice and lead to scattering centres, which decreases the carrier mobility [10,11]. Technical interest has been focused on developing high quality ITO crystalline films grown on single crystal substrates. For example, magnesium oxide (MgO), aluminium oxide (Al_2O_3), yttria-stabilised zirconia (YSZ), gallium arsenide (GaAs) and a zinc oxide (ZnO)-coated film on soda-lime glass have been employed to enhance the electrical properties of ITO [12–16]. Although the results of previous studies suggest that the preferred orientation can be achieved by altering the isotropic electrical properties of ITO films, significant differences in the electrical resistivity of the materials were not observed. Nevertheless, modulation-doping techniques used to fabricate AlGaAs/GaAs have been applied to ZnO/ZnO:Al films, and lower resistivities were obtained by separating the impurity-doped layer from the electron-conducting layer [17]. In the present study, a simple and low cost process was employed to improve the properties of ITO films, and a buffer layer of In_2O_3 was placed between the ITO film and the PES substrate. The structure of this sandwich-type film is designed as ITO/In_2O_3/substrate. The effects of the buffer film on the microstructure, electrical and optical properties of ITO films were investigated, and a correlation between the microstructure and the electrical and optical properties of ITO/In_2O_3 multilayered films was identified. For comparative purposes, single-layered ITO films without an In_2O_3 layer were prepared, and their properties were determined.

2. Experimental procedure

ITO and In_2O_3 thin films were prepared by RF-magnetron sputtering at room temperature. The ITO target (99.9% purity) was a commercially available hot-pressed pallet composed of 90 wt.% In_2O_3 with 10 wt.% SnO_2. The In_2O_3 target was made from pure In_2O_3 powder (Aldrich, 99.99%) and was sintered at 1500 °C for 4 h. The targets were 2 in. in diameter and presented a thickness of 3 mm. The In_2O_3 film was deposited on top of the PES substrate at sputtering times ranging from 5 to 35 min. Subsequently, the ITO film was deposited at a sputtering time of 5, 10 or15 min. The vacuum chamber was evacuated to a pressure of 10^{-6} Torr prior to the deposition process and was maintained at 5 mTorr during sputtering. The sputtering gas, which consisted of oxygen at a flow rate of 2 sccm, was carried by argon, and the RF power was set to 70 W. The deposition conditions of the samples are shown in Table 1. The crystal structure of the films was analysed by a X-ray diffractometer (Panalyical, X'pert Pro) with Cu Kα radiation (λ = 0.1542 nm), and the surface morphology and microstructure of the material were characterised by field emission scanning electron microscopy (FESEM, Philips, XL-40FEG). Transmission electron microscopy (TEM, FEI, Tecnai G^2) was used to determine the microstructure of reference material of a sample containing a glass substrate. The resistivity was measured according to the method of Van der Pauw, and optical transmittance measurements were collected at wavelengths of 300–900 nm using a UV/double-beam spectrophotometer.

Table 1
Sputtering conditions of the samples.

Film sample	Deposition time of ITO (min)	Deposition time of In_2O_3 (min)
Group A	5, 10, 15, 20, 25, 30, 35, 40	–
Group B	5	5, 10, 15, 20, 25, 30, 35
Group C	10	5, 10, 15, 20, 25, 30
Group D	15	5, 10, 15, 20, 25

3. Results and discussions

3.1. Characterisation of film microstructure

Fig. 1(a) shows the X-ray diffraction patterns of single-layer ITOs produced at different deposition times. As shown in the figure, the structure of the films was primarily amorphous during the early stages of ITO film growth. Thereafter, crystallisation occurred, and crystal growth along the (4 0 0) plane was observed as the sputtering time increased. Fig. 1(b) shows the XRD patterns of ITO/In_2O_3 multilayered films selected from groups B, C, and D deposited at a sputtering time of 40 min. Compared to single-layer ITO film, the crystallinity of ITO/In_2O_3 multilayered films was enhanced. In addition, the strongest crystallographic orientation shifted from (4 0 0) for single-layer ITO films in group A to (2 2 2) for multilayered films in groups C and D. The effect of the IO buffer layer on the crystallinity and crystal size of ITO films was determined according to the Scherrer formula [18]:

$$D = \frac{0.94\lambda}{\mathrm{FWHM}\cos\theta} \quad (1)$$

where D is the crystal size of the thin films, θ is the angle of the peak intensity and λ is the wavelength of the X-rays. The full width at half maximum (FWHM, the width of the peak at half the maximum peak intensity) is inversely proportional to the crystal size and is related to the degree of crystallinity in columnar polycrystalline thin films [19]. Figs. 2 and 3 show the FWHM values at 2θ for the (2 2 2) diffraction peaks and the corresponding crystal sizes of the films as a function of the total deposition time. As shown in the figure, as the total deposition time of the films increased, the FWHM value decreased and the crystal size increased. Nevertheless, multilayered films displayed superior crystallinity and larger grain sizes than single-layer ITO films.

Fig. 4 shows FESEM images of selected samples from groups A, B, C and D deposited at a sputtering time of 40 min. The grain size obtained from the FESEM image was comparable to the XRD data, which were calculated according

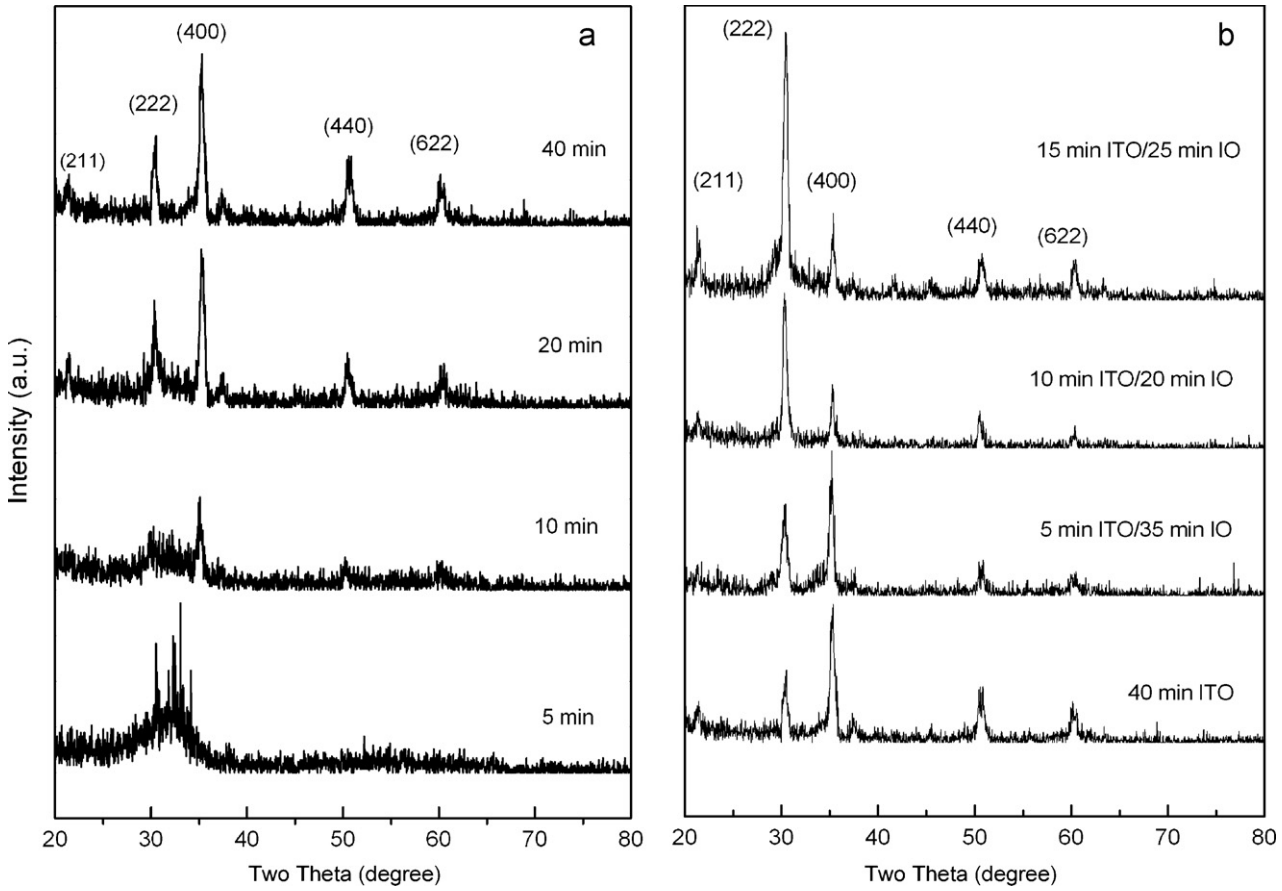

Fig. 1. X-ray diffraction patterns of (a) single-layered ITO films and (b) ITO/In_2O_3 multilayered films deposited at room temperature at various deposition times.

to the Scherrer formula. Thus, the results confirmed that the crystallinity and crystal size of ITO/In_2O_3 multilayer films were enhanced by the deposition of an In_2O_3 buffer film. The crystal size of the ITO layer increased from 20 nm to 45 nm for ITO/In_2O_3 multilayered films.

The microstructure of ITO/In_2O_3 multilayered films was also examined by TEM. Fig. 5(a) shows a cross-sectional image of a sample that was produced by depositing a film of In_2O_3 and ITO for 15 and 25 min, respectively. Two distinct layers separated by a zigzag-type interface were observed between the ITO and In_2O_3 film. X-ray analysis verified the presence of indium and tin in the ITO film (top layer). In contrast, tin was not detected in the In_2O_3 film (bottom layer). TEM analysis confirmed the results of the XRD investigation, indicating that the (2 2 2) planes in the multilayer film were highly oriented, forming a columnar

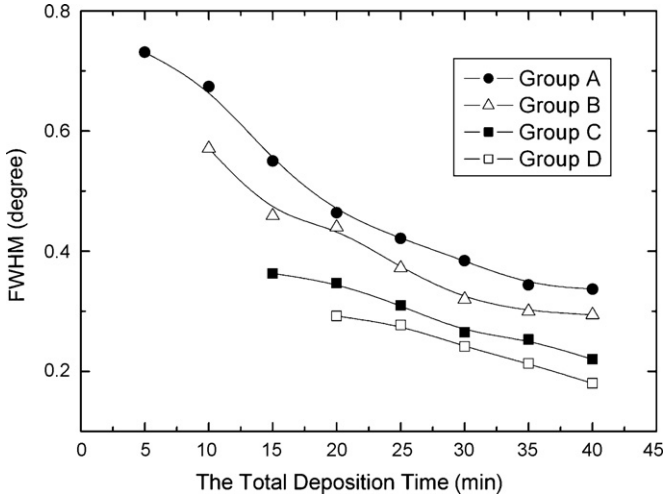

Fig. 2. FWHM of the film as a function of the total deposition time.

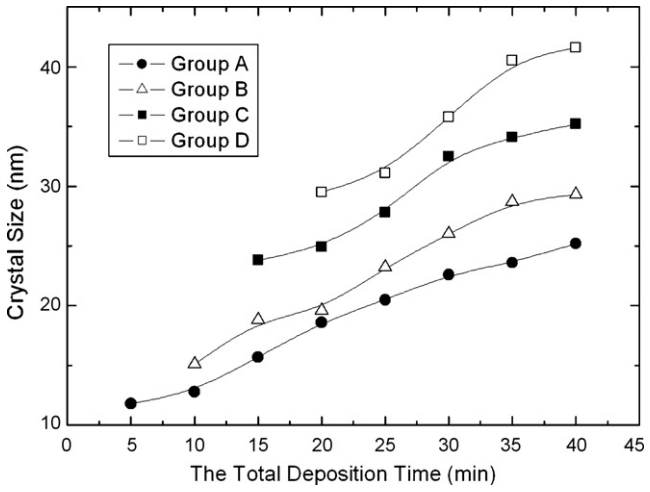

Fig. 3. Crystal size of the film as a function of the total deposition time.

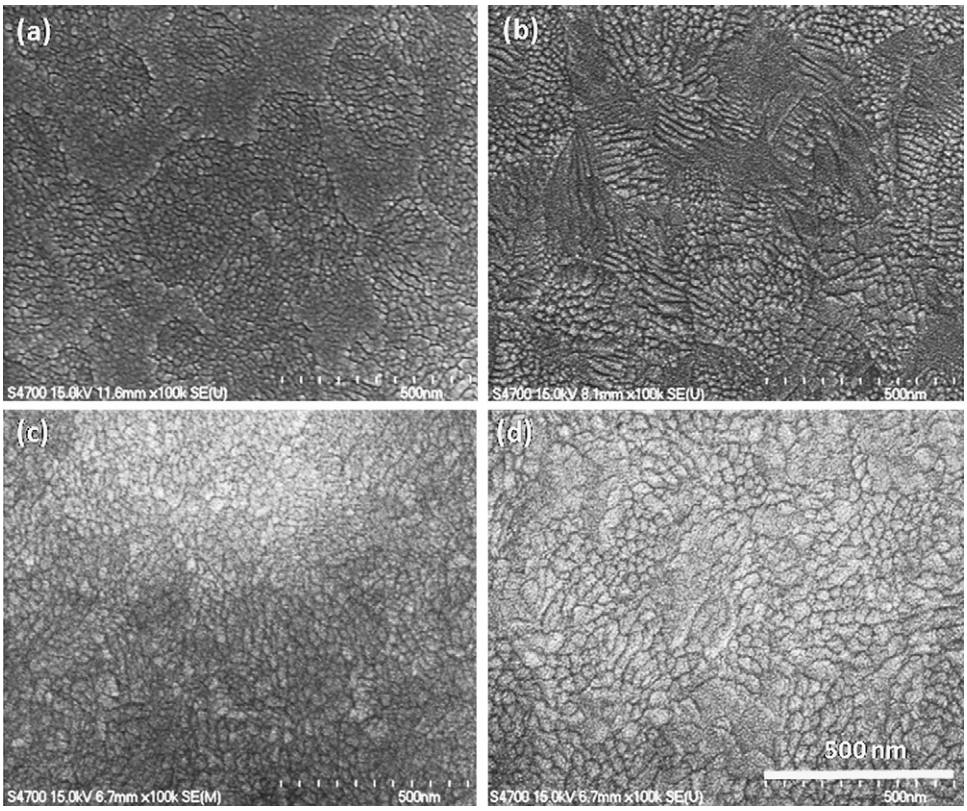

Fig. 4. FESEM images of films deposited at a total deposition time of 40 min for (a) single-layered ITO film, (b) 5 min ITO/35 min In_2O_3, (c) 10 min ITO/25 min In_2O_3 and (d) 15 min ITO/25 min In_2O_3 multilayered films.

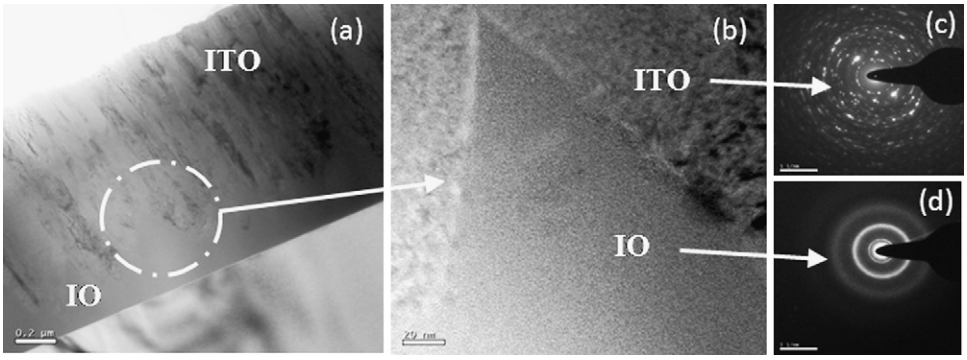

Fig. 5. (a) TEM images of 15 min ITO/25 min In_2O_3 multilayered films deposited at a total deposition time of 40 min. (b) Enlarged image of (a). (c and d) The SAD patterns of ITO and In_2O_3 films.

texture. The growth of crystalline transparent conducting films on an amorphous phase has been reported in previous studies [20,21], and a similar vertical columnar structure was observed by Kulkarni et al. [22]. Fig. 5(b) shows an enlarged image of Fig. 5(a), and Fig. 5(c) and (d) displays selected area electron diffraction (SAD) patterns collected from the ITO and In_2O_3 regions of a multilayered film, respectively. The SAD pattern of the ITO film revealed a series of distinct rings representing the order of atomic distance. Although the SAD of the In_2O_3 film exhibited diffuse halos, the high resolution electron image further revealed that the film displayed short-range order and was composed of 1–3-nm crystallites.

3.2. Evaluation of the electrical and optical properties of the films

The electrical resistivity of ITO/In_2O_3 multilayered and ITO single-layered films at room temperature was plotted as a function of the total deposition time, and the results are shown in Fig. 6. The data clearly indicated that the electrical resistivity of the films decreased with an increase in the total deposition time. However, the properties of the films stabilised when a certain deposition time was attained. In the early stages of the deposition process, the density of grain boundaries was higher due to the smaller grain size, formation of islands and presence of voids, which were attributed to the higher electrical

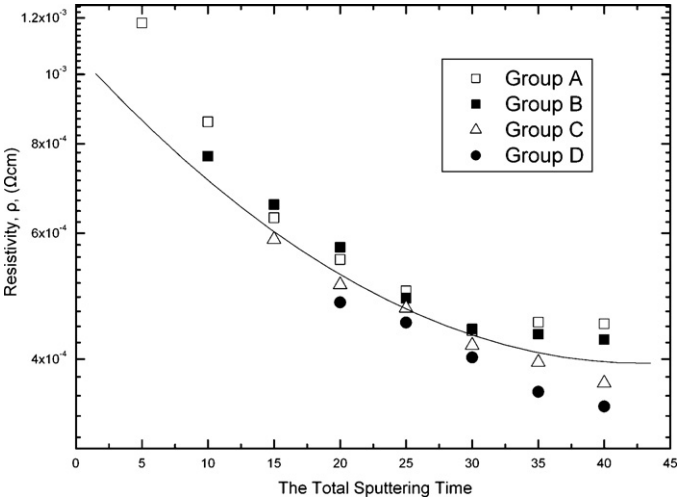

Fig. 6. Electrical resistivity of selected films from groups A, B, C and D as a function of the total deposition time.

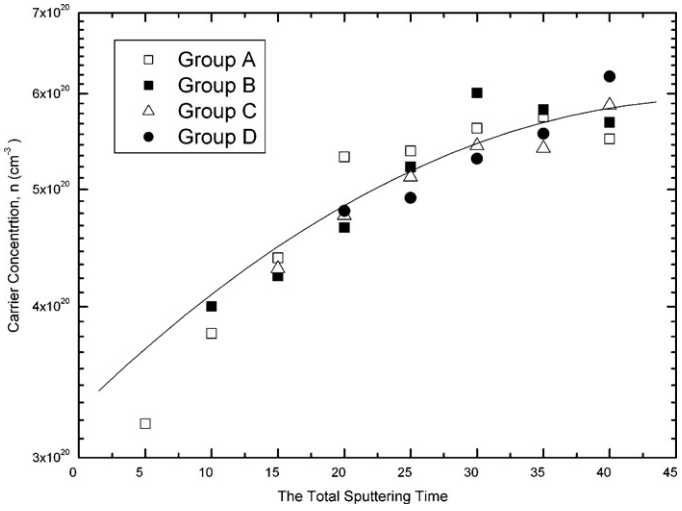

Fig. 7. Carrier concentration of selected films from groups A, B, C and D as a function of the total deposition time.

resistivity. As the deposition time increased, a sudden onset of resistivity was detected. The observed decrease in resistivity was correlated to an increase in the carrier concentration and mobility. The carrier concentration and mobility as a function of the total deposition time are plotted in Figs. 7 and 8. For all of the films, the carrier concentration increased with an increase in the total deposition time due to the bombardment of high energetic particles on the films, which promoted the substitution of Sn^{4+} into the indium sites of the In_2O_3 lattice, creating a free electron. Thus, due to the donor electron from Sn, the initial increase in the carrier concentration decreased the resistivity. However, after 30 min of deposition, the carrier density of the films reached a saturated value of 6×10^{22} cm^{-3} and began to decrease for single-layer ITO films. As the deposition time increases, excess doping may occur, allowing Sn to occupy interstitial positions or to form defects such as SnO, Sn_2O and Sn_2O_4, which act as carrier traps rather than electron donors [23].

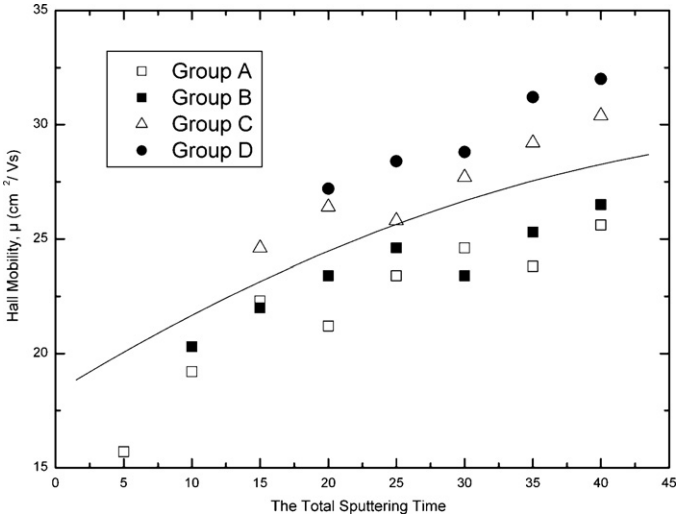

Fig. 8. Hall mobility of films from groups A, B, C and D as a function of the total deposition time.

As shown in Fig. 8, the Hall mobility increased gradually with an increase in the total deposition time. The mobility of films is strongly influenced by the disorder of the ITO structure, especially during the early stages of the deposition process. Therefore, the Hall mobility of films with high degrees of crystallinity was expected to increase with an increase in the deposition time due to the relatively large crystal size and low grain boundary scattering. Due to the effect of the In_2O_3 buffer layer, the resistivity of multilayered films was lower than that of films without an In_2O_3 buffer layer; however, an obvious improvement was not observed in group B. Nevertheless, at a fixed deposition time, thicker films or materials produced at longer deposition times showed lower electrical resistivity. In most cases, the following trend in the electrical resistivity was observed: group D < group C < group A. For example, at a total deposition time of 40 min, multilayered films in group D (15 min ITO/25 min In_2O_3) presented a resistivity of $3.1 \times 10^{-4}\ \Omega$ cm, which was lower than that of single-layer ITO films in group A ($4.7 \times 10^{-4}\ \Omega$ cm). As a result, films in group A possessed a higher mobility (32.1 cm^2/Vs) than that of single-layer ITO films (25.6 cm^2/Vs). The observed decrease in resistivity due to the application of an In_2O_3 buffer film between the ITO film and the substrate was attributed to an improvement in the crystallinity and crystal size of the ITO film, as evidenced by the XRD and FESEM results. The high crystallinity of these films is associated with an enhancement in the surface mobility of atoms [24], which improves nucleation and the annealing of defects during film growth, resulting in superior surface morphology. Therefore, the electrical resistivity of films decreased due to an improvement in the doping efficiency and a reduction in scattering. In previous studies, the properties of ITO and AZO films were improved by applying a ZnO buffer layer [17,25].

The optical transmittance spectra of ITO/In_2O_3 multilayer films and single-layer ITO produced at a deposition time of 40 min are shown in Fig. 9. For comparison, a single-layer ITO film produced at a deposition time of 10 min is also presented in

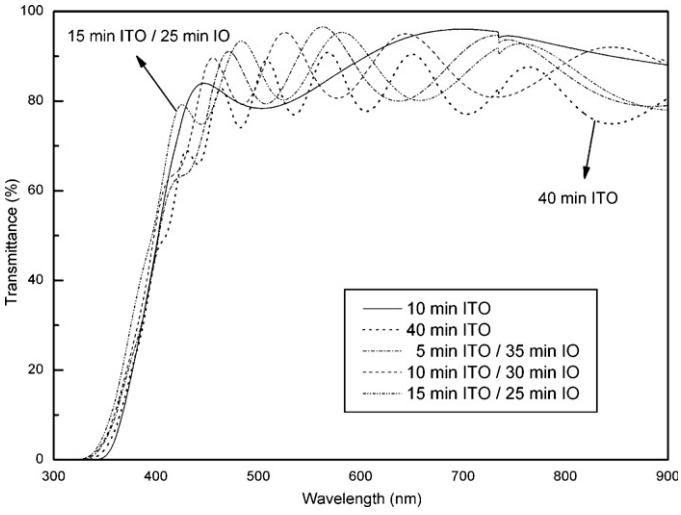

Fig. 9. Optical transmittance spectra of selected films from groups A, B, C and D.

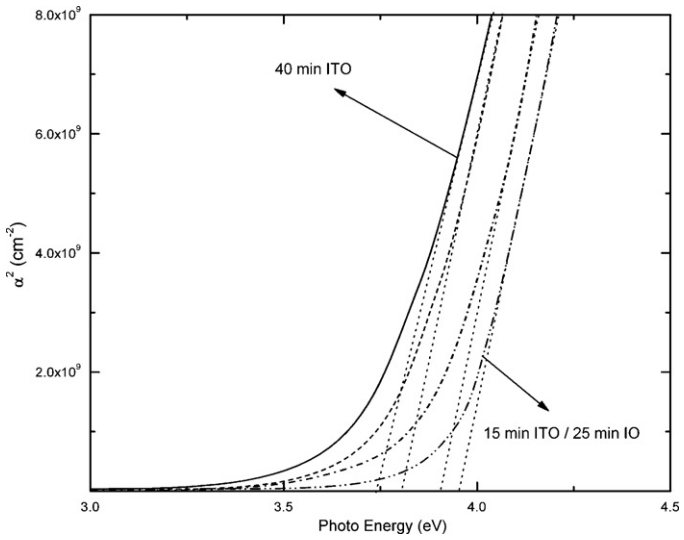

Fig. 10. Square of the absorption coefficient, α^2, as a function of the photon energy of the samples shown in Fig. 9.

the figure. All of the films displayed an average transmittance of 80–85%. However, the transmittance of ITO/In_2O_3 multilayer films was greater than that of single-layer ITO films due to the homogeneous microstructure, larger grain size and lower defect density of multilayered films. When the film was relatively thin or was produced at a shorter deposition time, the transmittance minimum due to destructive interference was located at a wavelength of 500 nm. As an example, the single-layer ITO film produced at a deposition time of 10 min is shown in Fig. 8. However, as the film thickness or deposition time increased, the wavelength of the local transmittance maximum and minimum ranged from 500 to 900 nm. The observed oscillation in the optical transmission spectra was attributed to the thickness of the film and to interference between multiple internal reflections among ITO/In_2O_3 and In_2O_3/substrate interfaces. The most significant difference in the transmittance curves of the materials was observed in the threshold of optical absorption. Namely, the threshold of multilayered films was shifted to shorter wavelengths; thus, the band gap increased due to an increase in the carrier concentration of the film. The optical properties of ITO films are related to free carrier absorption and can be expressed by Drude theory [26]. Using the transmittance and reflectance data, the absorption coefficient (α) of the films was calculated according to the following expression:

$$I = I_0 e^{-\alpha d} \tag{2}$$

where I is the intensity of transmitted light, I_0 is the intensity of incident light and d is the thickness of the film. Using the following relationship, the absorption coefficient data were used to determine the energy gap (E_g):

$$\alpha h\nu \approx (h\nu - E_g)^{1/2} \tag{3}$$

where $h\nu$ is the photon energy. In Fig. 10, α^2 is plotted against the photon energy of the films shown in Fig. 9. The values of the direct optical band gap, E_g, were determined by extrapolating the linear region of the plots to zero absorption. The results suggested that the direct band gap of single-layered ITO film produced at a deposition time of 40 min was 3.72 eV, and the direct band gap of the 15 min ITO/25 min In_2O_3 multilayered film was 3.93 eV. The observed widening of the band gap was attributed to a Burstin–Moss shift [27,28]. According to Burstin–Moss theory, the lowest states of the conduction band are occupied by free electrons, and valence electrons require extra energy to be excited to higher energy states within the conduction band. Therefore, the optical band gaps of multi-layered ITO films are wider than that of single-layered ITO films. Indeed, the optical spectra results verified the Hall measurement data and suggested that the carrier concentrations of multilayer films were greater than those of single-layer films.

4. Summary

An improvement in the electrical resistivity of ITO films was achieved by applying an In_2O_3 buffer layer between the ITO film and the PES substrate. For example, the resistivity of the films decreased from $4.7 \times 10^{-4}\ \Omega$ cm to $3.1 \times 10^{-4}\ \Omega$ cm when an In_2O_3 buffer layer produced at a deposition time of 25 min was applied. The observed improvement in the electrical conductivity was attributed to enhanced crystallisation. XRD and FESEM analysis indicated that multilayered thin films displayed superior crystallinity and larger crystal size. For instance, when an In_2O_3 buffer layer was employed, the crystal size of the film increased from 20 to 45 nm. As a result, superior doping efficiency and less scattering were observed, and a carrier concentration of 6.2×10^{20} cm^{-3} and a Hall mobility of 32.1 cm^2/Vs were obtained. Although the optical transmittance of multilayer films was similar to that of single-layer ITO films, the absorption edge of multilayered ITO/In_2O_3 films shifted towards higher wave numbers due to a higher carrier concentration.

Acknowledgement

The authors are grateful to the National Science Council of Taiwan for financial support (grant no. 95-2745-E-214-002).

References

[1] R. Barber, G. Pryor, E. Reinheimer, Designing for Electromagnetic Compatibility, DIS Digest of Tech. Papers 28, 1997, p. 18.
[2] K. Moschovis, E. Gagaoudakis, E. Chatzitheodordis, G. Kiriakidis, S. Mailis, E. Tzamali, N.A. Vainos, H. Fritzsche, Study of the ambient optical recording dynamics on sputtered indium oxide thin films, Appl. Phys. A 66 (1998) 651–654.
[3] B.G. Lewis, D.C. Paine, Application and processing of transparent conducting oxides, MRS Bull. 25 (2000) 22–27.
[4] I. Nakamura, M. Kamiya, I. Takano, Y. Sawada, E. Nakazawa, Formation of In–O films by Ar^+ ion beam assisted reactive deposition, Surf. Coat. Technol. 103–104 (1998) 83–86.
[5] H. Kim, J.S. Horwitz, G. Kushto, A. Pique, Z.H. Kafafi, C.M. Gilmore, D.B. Chrisey, Effect of film thickness on the properties of indium tin oxide thin films, J. Appl. Phys. 88 (2000) 6021–6025.
[6] K. Utsumi, O. Matsunaga, T. Takahata, Low resistivity ITO film prepared using the ultra high density ITO target, Thin Solid Films 334 (1998) 30–34.
[7] T. Minami, T. Yamamoto, T. Miyata, Highly transparent and conductive rare earth-doped ZnO thin films prepared by magnetron sputtering, Thin Solid Films 366 (2000) 63–68.
[8] M. Fahland, P. Karlsson, C. Charton, Low resistivity transparent electrodes for displays on polymer substrates, Thin Solid Films 392 (2001) 334–337.
[9] E. Fortunato, P. Nunes, D. Costa, D. Brida, I. Ferreira, R. Martins, Characterization of aluminium doped zinc oxide thin films deposited on polymeric substrates, Vacuum 64 (2002) 233–236.
[10] S.B. Lee, J.C. Pincenti, A. Cocco, D.L. Naylor, Electronic and optical properties of room temperature sputter deposited indium tin oxide, J. Vac. Sci. Technol. A 11 (1993) 2742–2746.
[11] B.G. Choi, I.H. Kim, D.H. Kim, K.S. Lee, T.S. Lee, B. Cheong, Y.J. Baik, W.M. Kim, Electrical, optical and structural properties of transparent and conducting ZnO thin films doped with Al and F by RF magnetron sputter, J. Eur. Ceram. Soc. 25 (2005) 2161–2165.
[12] M. Kamei, Y. Shigesato, S. Takaki, Origin of characteristic grain–subgrain structure of tin-doped indium oxide films, Thin Solid Films 259 (1995) 38–45.
[13] J.C.C. Fan, F.J. Bachner, Properties of Sn-doped In_2O_3 films prepared by RF sputtering, J. Electrochem. Soc. 122 (1975) 1719–1724.
[14] V. Lisauskas, R. Butkuté, L. Dapkus, A. Jukna, B. Vengalis, Preparation of epitaxial indium-tin oxide films on ZrO_2 substrates by magnetron sputtering, Lith. Phys. J. 36 (1996) 104–107.
[15] E.J. Tarsa, J.H. English, J.S. Speck, Pulsed laser deposition of oriented In_2O_3 on (0 0 1) InAs, MgO, and yttria-stabilized zirconia, Appl. Phys. Lett. 62 (1993) 2332–2334.
[16] C.H. Yi, I. Yasui, Y. Shigesato, Oriented tin-doped indium oxide films on ⟨001⟩ preferred oriented polycrystalline ZnO films, Jpn. J. Appl. Phys. 134 (1995) 1638–1642.
[17] K. Tominaga, N. Umezu, I. Mori, T. Ushiro, T. Moriga, I. Nakabayashi, Transparent conductive ZnO film preparation by alternating sputtering of ZnO:Al and Zn or Al targets, Thin Solid Films 334 (1998) 35–39.
[18] B. Cullity, Elements of X-ray Diffraction, Addison-Wesley, 1978,, p. 102.
[19] H. Kim, C.M. Gilmor, Electrical, optical, and structural properties of indium-tin-oxide thin films for organic light-emitting devices, J. Appl. Phys. 86 (1999) 6451–6461.
[20] E. Fortunato, P. Nunes, D. Costa, D. Brida, I. Ferreira, R. Martins, Characterization of aluminum doped zinc oxide thin films deposited on polymeric substrates, Vacuum 64 (2002) 233–236.
[21] S.K. Park, J.I. Han, W.K. Kim, M.G. Kwak, Deposition of indium-tin-oxide films on polymer substrates for application in plastic-based flat panel displays, Thin Solid Films 397 (2001) 49–55.
[22] A.K. Kulkarni, K.H. Schlz, T.S. Lim, M. Khan, Electrical, optical and structural characteristics of indium-tin-oxide thin films deposited on glass and polymer substrates, Thin Solid Films 308–309 (1997) 1–7.
[23] R.B.H. Tahar, T. Ban, Y. Ohya, Y. Takahashi, Tin doped indium oxide thin films: electrical properties, J. Appl. Phys. 83 (1998) 2631–2645.
[24] J.A. Thornton, J.E. Greene, Handbook of Deposition Technologies for Films and Coating, 2nd edition, Noyes, Park Ridge, NJ, 1994.
[25] X.W. Sun, L.D. Wang, H.S. Kwok, Improved ITO thin films with a thin ZnO buffer layer by sputtering, Thin Solid Films 360 (2000) 75–81.
[26] H.L. Hartnagel, A.L. Dawar, A.K. Jain, C. Jagadish, Semiconducting Transparent Thin Films, Institute of Physics Publishing, Philadelphia, 1995.
[27] E. Burstein, Anomalous optical absorption limit in InSb, Phys. Rev. 93 (1954) 632–633.
[28] T.S. Moss, The interpretation of the properties of indium antimonide, Proc. Phys. Soc. B 67 (1964) 775–782.